Design of a Reconfigurable Force Feedback Ankle Exoskeleton for Physical Therapy

Ahmetcan Erdogan [1], Aykut Cihan Satici [1], Volkan Patoglu [1]

[1] Faculty of Engineering and Natural Sciences
Sabancı University
İstanbul, Turkey
{ahmetcan,acsatici}@su.sabanciuniv.edu
vpatoglu@sabanciuniv.edu

Abstract—*This paper presents the design and the optimal dimensional synthesis of a reconfigurable, parallel mechanism based, force feedback exoskeleton for the human ankle. The primary use for the device is aimed as a balance/proprioception trainer, while the exoskeleton can also be employed to accommodate range of motion (RoM)/strengthening exercises. Multiple design objectives for several physical therapy exercises are discussed and classified for the design of the rehabilitation device. After kinematic structures of mechanisms that are best suited for the physical therapy applications are selected, an optimization problem to study the trade-offs between multiple design criteria is formulated. Dimensional synthesis is performed to achieve the maximum stiffness of the device, while simultaneously maximizing the actuator utilization, using a Pareto-front based framework. An "optimal" design is selected studying the Pareto-front curve and taking the primary and secondary design criteria into account. Once the dimensions of the device are decided, reconfigurability is built into the design such that the device can be arranged as a 3UPS manipulator to administer RoM/strengthing exercises and as a 3RPS manipulator to support balance/proprioception training. Metatarsophalangeal joint exercises are also enabled through a reconfigurable design of the foot plate. Details of the final design of the ankle exoskeleton, CAD snapshots, and an early prototype of the device are also presented.*

Index Terms—*Reconfigurable Mechanisms, Reconfigurable Robots.*

1. Introduction

Assistance of repetitive and physically involved rehabilitation exercises using robotic devices not only helps eliminate the physical burden of movement therapy for the therapists, but also decreases application related costs. Moreover, robot-mediated rehabilitation therapy allows quantitative measurements of patient progress and can be used to realize customized, interactive treatment protocols. In this article, we develop a novel rehabilitation exoskeleton for patients who have suffered injuries that impair the function of their lower extremities, specifically their ankle and foot movements.

The aim of rehabilitation is to recover the patient's physical, sensory and neural capabilities that were impaired due to an illness or injury. Ankle rehabilitation is commonly necessitated after sprained ankles, one of the most common injuries in sports and daily life [1]. Loss of functional ability, ability to bear weight, and joint stability at the ankle are also experienced after neurological injuries secondary to stroke and contracture deformity secondary to cerebrovascular disease. Physiotherapy exercises are indispensable to re-gain range of motion (RoM) of the joint, to help restrengthen muscles to bear weight, to promote better awareness of joint position (proprioception), to ensure neural integrity, and to recover dynamic balance.

Rehabilitation of ankle injury is generally addressed in three sequential exercise phases [2], [3]. Exercises in the early phase focus on first enabling full RoM of the joint and then strengthening ankle muscles. Once the required RoM and flexibility is achieved and the muscles become strong enough to bear partial weight without inducing pain, the intermediate phase of therapy can be initiated, focusing on the enhancement of proprioception ability through use of static balance exercises. In the final phase of the therapy, more advanced dynamic balancing exercises are practiced.

Traditional rehabilitation devices used to assist physiotherapy are simple passive equipment, such as elastic bands and ankle rehabilitation pumps for strengthening and stretching exercises; wobble boards and foam rollers for proprioception and balancing exercises. RoM exercises are generally performed manually by a therapist. Even though these equipment are simple and fixed-cost effective, these traditional devices fall short of collecting quantitative measurements of patient progress, monitoring patient history for re-evaluation, and achieving customized, interactive treatment protocols. The therapists are required to carry physical burden of movement therapy and to provide the patient with full attention while exercising with these devices.

Beneficial effects of robot assisted rehabilitation protocols have been demonstrated over conventional therapy through clinical trials in the literature [4]. Recognizing the need for robot assisted rehabilitation devices for ankle physiotherapy, several designs have been proposed to date. Girone *et al.* proposed a force feedback interface, named Rutgers Ankle, based on Stewart platform [5]. In [6], a virtual reality based interactive training protocol was implemented using the Rutgers Ankle for orthopedic rehabilitation. The system was further studied in [7] and [8] through several case studies. Home-based remote ankle rehabilitation was addressed in [9], while in [10] the system was extended to a dual Stewart platform configuration to be used for gait simulation and rehabilitation.

I.S. Dai, M. Zoppi and X. Kong (eds.), ASME/IFToMM International Conference on Reconfigurable Mechanisms and Robots

In [11], Dai *et al.* proposed another robotic device to treat sprained ankle injuries. Unlike the Stewart platform based design, this device possesses just enough degrees of freedom (DoF) to cover the orientation workspace of the human ankle. The kinetostatic analysis presented in this reference emphasized the importance of employing a center strut to achieve higher stiffness from the device. In [12], Agrawal *et al.* proposed an ankle-foot orthosis for robot assisted rehabilitation and presented the kinematic analysis and the control of the proposed mechanism. Similarly, in [13] Anklebot was proposed by Roy *et al.* to aid recovery of the ankle function. This device can also be used to measure the ankle stiffness, which is a strong biomechanical factor for locomotion.

Syrseloudis and Emiris studied the translational and rotational RoM of human ankle and foot through human subject experiments, and concluded that a parallel tripod mechanism with an additional rotational axis in series is the most relevant kinematic design to comply with human ankle related foot kinematics [14]. In [15] Yoon and Ryu proposed an hybrid four DoF parallel mechanism based footpad device and presented the kinematic analysis of the novel device. In [3] and [16], this work was extended to allow for reconfiguration of the device to support several distinct exercise modes.

In this article, the design and optimal dimensional synthesis of a reconfigurable, parallel mechanism based ankle exoskeleton are presented. Similar to references [3] and [16], reconfigurability is built into the design such that the device can be arranged to administer ROM/strengthing exercises and to support balance/proprioception exercises. Metatarsophalangeal (MTP) joint exercises are also enabled via the reconfigurable design of the foot plate. The kinematic structures of the exoskeletons are carefully selected after identifying the relevant design criteria for several physical therapy exercises. Similar to all of the cited references, parallel mechanisms are employed for the design due to their inherent advantages. However, unlike any of the existing designs, a 3U$\underline{\text{P}}$S[1] mechanism is proposed to be the most suitable for RoM/strengthening exercises, while a 3R$\underline{\text{P}}$S mechanism (with a passive revolute joint in series) is proposed to support balance/proprioception exercises.

The paper is organized as follows: Section 2 introduces the kinematic model of human ankle and discusses the selection two distinct parallel mechanisms as the kinematic structures to be employed in two distinct exercise modes. Several design objectives are identified and categorized in Section 3. Section 4 formulates the multi-criteria optimization problem, explains the solution method used to address the problem, and presents the implementation and results of the optimal dimensional synthesis. Section 5 discusses the implementation details of the reconfigurable exoskeleton device. Finally, Section 6 concludes the paper.

[1]Parallel mechanisms are commonly denoted by using symbols U, R, S, and P, which stand for universal, revolute, spherical, and prismatic joints. Symbols corresponding to actuated joints are underlined in this notation.

TABLE I
WORKSPACE AND TORQUE LIMITS OF HUMAN ANKLE

Joint	Joint Torque Limits	Designed Torque Limits	Joint RoM	Designed RoM
Dorsiflexion\ Plantarflexion	40.7–97.6 Nm 20.3–36.6 Nm	100 Nm 50 Nm	20° 40°	40° 40°
Inversion\ Eversion	max 48 Nm max 34 Nm	50 Nm 50 Nm	35° 25°	35° 35°

TABLE II
FOOT MEASUREMENT DATA

Body part	5^{th} percentile	95^{th} percentile
Ankle circumference	200 mm	248 mm
Ball of foot circumference	229 mm	275 mm
Bimalleolar breadth	67 mm	81 mm
Calf circumference	336 mm	432 mm
Calf height	316 mm	405 mm
Foot breadth	92 mm	111 mm
Foot length	249 mm	298 mm
Heel-ankle circumference	313 mm	375 mm
Heel breadth	62 mm	82 mm
Kneecap (patella) height	468 mm	569 mm
Lateral malleolus height	58 mm	78 mm
Medial malleolus height	76 mm	97 mm

2. KINEMATICS OF HUMAN ANKLE AND ANKLE EXOSKELETON

Kinematics of the human ankle, which allows plantarflexion/dorsiflexion, abduction/adduction, and inversion/eversion of the foot is quite complex. Many studies make use of a simplified three DoF spherical joint model for the ankle joint, in which the axes of rotation for these three motions are assumed to coincide at a single point on the ankle [11], [17]. In this study, the kinematics of the human ankle is presumed to comply with a biomechanics model that is verified by and commonly utilized in the literature [14]. This model recognizes the coupled motion of the foot and hypothesizes that the ankle joint can be modeled as a serial kinematic chain with two revolute joints (RR): an upper ankle joint that supports the rotational dorsiflexion/plantarflexion motion and a subtalar joint that supports the rotational supination/pronation motion. Supination/pronation is a complex motion which has both inversion/eversion and abduction/adduction components. The exact motion of the ankle shows wide variation among humans as this motion depends on size and orientation of foot bones, shape of articulated surfaces and constraints imposed by ligaments, capsules, and tendons. Workspace and torque limits of human ankle are given in Table I based on [3]. Similarly statistical data on human foot and ankle sizes is summarized in Table II [18].

A kinematic chain that is suitable to serve as an exoskeleton should allow for and support natural movements of the human joints when the device is worn by an operator. To ensure safety, to allow for joint misalignments and modeling imperfections, couplings between the exoskeleton and the operator are designed to be elastic. Elasticity allows for the relative motion of the human limb with respect to the device when the kinematics of the device is in conflict with the natural motion of the ankle.

However, it is still desirable to have the exoskeleton to possess kinematics that is compatible with the human ankle motions so that the motion of the ankle can be closely controlled during the therapy. Hence, kinematic structures that closely meet the ergonomy requirement are preferred.

Once the ergonomy requirement is met, the choice of closed kinematic chains (parallel mechanisms) is preferable over the choice of serial mechanisms in satisfying requirements of force feedback applications, for a number of reasons. Specifically, parallel mechanisms offer compact designs with high stiffness and have low effective inertia since their actuators can be grounded or placed on parts of the mechanism that experience low accelerations. In terms of dynamic performance, high position and force bandwidths are achievable with parallel mechanisms thanks to their light but stiff structure. Besides, parallel mechanisms do not superimpose position errors at joints; hence, can achieve high precision.

In order to span the whole natural range of motion of the human ankle and to do so robustly for various operators of different ankle and foot dimensions (kinematics), an underactuated 3UPS parallel mechanism is proposed as the kinematic structure of the exoskeleton. A 3UPS mechanism has six DoF that can be designed to cover all RoM of the human ankle and foot. Having only three actuators, the 3UPS mechanism is not of much use by itself; however, when worn by a human operator, the kinematics of the human ankle becomes a part of the exoskeleton. Coupled to the human operator, the 3UPS exoskeleton operates as a 3UPS-RR kinematic structure with two independent degrees of freedom, dictated by the kinematics of the human ankle. Hence, not only can the device cover the RoM of any operator, but can do so in a completely ergonomic manner. Moreover, even when the operator is completely passive, the two DoF 3UPS-RR device has three actuated joints and is a redundant mechanism. This redundancy can be used as an advantage, especially when the device approaches kinematic singularities within its workspace.

Employing the human ankle as a part of the kinematic chain, the 3UPS-RR configuration is useful for RoM/strengthing exercises; however, this kinematic structure is not preferable for balance/proprioception exercises, since the forces/torques transferred to the ankle joint cannot be supported. To support to the human weight and to adjust the torques transferred to the ankle joints while covering an acceptable portion of the natural human ankle workspace, a 3RPS-R parallel mechanism is proposed as the kinematic structure of the exoskeleton. The 3RPS-R mechanism has four DoF. Three of these DoF, actuating the 3RPS part of the mechanism, are controlled using prismatic actuators. The kinematics of the 3RPS-R mechanism can closely approximate the natural motion of the human ankle. When worn by an operator, 3RPS-R mechanism can dictate the motion of the human ankle though elastic couplings. The three DoF 3RPS can be easily programmed to trace trajectories that closely approximate the natural movements of the human ankle. The passive revolute joint at the base platform of the 3RPS-R allows for the internal/external rotations of the foot and recovers most of the useful workspace during balancing exercises.

In this paper, a reconfigurable mechanism that can serve both as the 3RPS-R and the 3UPS mechanism is selected to represent the kinematics of the ankle exoskeleton. Both of these mechanisms belong to the family of parallel mechanisms. Even though there have been important recent advances in the type synthesis of parallel mechanisms [19], [20], [21], many of even the most basic types are yet to be analyzed in detail [22]. 3UPS-RR and 3RPS mechanisms are among the few parallel mechanisms, whose kinematic and singularity analyses have been addressed in the literature. Moreover, being compact and allowing for human ankle motions without collisions with the device, these two mechanisms are the most suitable parallel mechanisms to serve as wearable force feedback devices. The 3RPS and the 3UPS-RR mechanisms are depicted in Figure 1.

The 3RPS platform, first introduced by Lee *et al.* [23], and further analyzed in [24], consists of five bodies: a base platform F, three extensible links R, S, T, and a moving platform W. The end-effector elastically coupled to the operator is attached to the moving platform W. Extensible links are connected to the base platform via revolute joints whose axes of rotation are oriented along the tangents of F, while the moving platform is connected to the extensible links by means of spherical joints. In our implementation, the base platform F is attached to the upper mid-calf of the leg N through a passive revolute joint to allow for the internal/external rotations of the foot. In this paper, the analysis is limited to a symmetric 3RPS mechanism where the revolute joints and the spherical joints are spaced at 120° along the circumference of the base platform of radius R and the moving platform of radius r, respectively.

The 3RPS mechanism has three DoF corresponding to the height z and two Euler angles Ψ_1, Ψ_2 of the moving platform W with respect to the Newtonian reference frame N. The lengths of the extensible links are actuated to control these DoF. The platform possesses limited translational movement transverse to the vertical axis through the base and no singularities for limited values of revolute joint angles $\theta_i \in (0, \pi/2)$ [23]. The 3RPS mechanism is first utilized as a wrist exoskeleton device by Gupta *et al.* [25] and adapted as a wrist rehabilitation device in [26]. The optimal design of 3RPS mechanism for force feedback applications is addressed in [27] and [28].

The 3UPS-RR mechanism consists of six bodies: a base platform N, three extensible links R, S, T, a center link A, and a moving platform W. The end-effector worn by the operator; hence, the foot, is elastically attached to the moving platform W. The ankle of the operator is idealized as two revolute joints in series (RR) and the upper mid-calf of the operator is fixed to the base platform N. Hence, for this mechanism, the human ankle counts as a part of the kinematic structure. Extensible links are connected to the base platform via universal joints, while the rotating platform is connected to the extensible links by means of spherical joints. In this paper, the analysis is limited to a symmetric 3UPS-RR mechanism

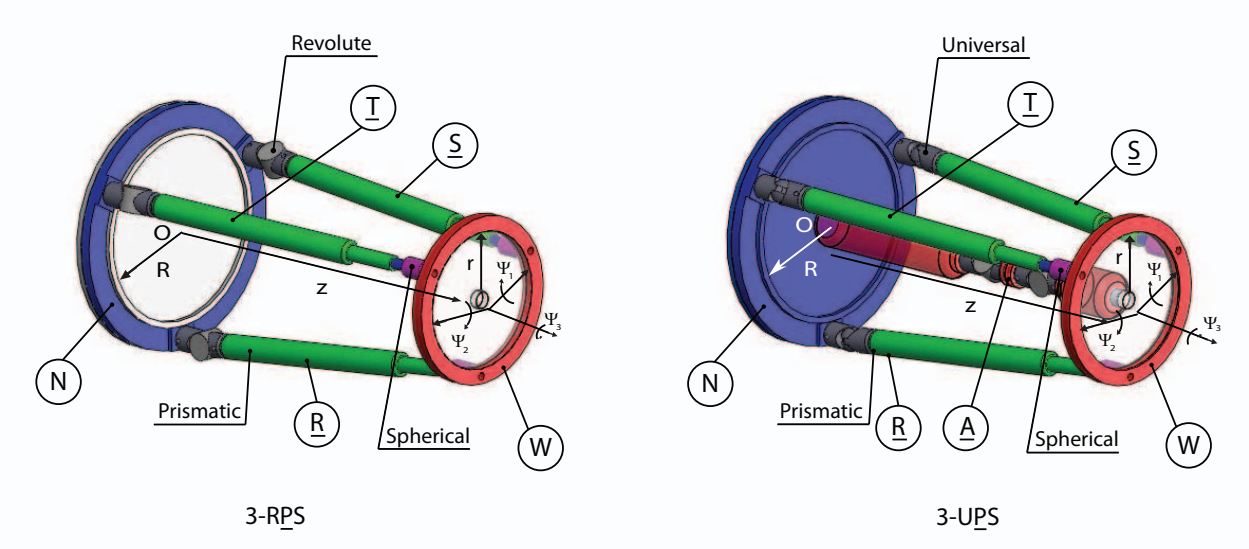

Fig. 1. 3RPS and 3UPS mechanisms in perspective views

where the universal joints and the spherical joints are spaced at 120° along the circumference of the base platform of radius R and the moving platform of radius r, respectively.

The 3UPS-RR mechanism has two DoF corresponding to a coupled motion of the moving platform W with respect to the fixed reference frame N. The lengths of the extensible links are actuated to control these DoF. The moving platform is a distance z from the base platform and does not possess translational movement transverse to the vertical axis through the base. Even when human operator is completely passive, the two DoF 3UPS-RR structure has three actuated joints; hence, is a redundant mechanism. This redundancy can be exploited to increase the effective workspace of the device, since singularity resolution becomes feasible in case the device approaches kinematic singularities within its workspace.

Since the performance of parallel mechanisms is highly sensitive to their dimensions, optimization studies are absolutely necessary for design of these types of mechanisms [29]. In this paper, optimal dimensions for the reconfigurable ankle exoskeleton mechanisms are calculated with respect to multiple design criteria to be detailed in the next section.

3. Design Objectives

Following the terminology of Merlet [29], one can categorize the performance requirements of a mechanism into four distinct groups: *Imperative* requirements that must be satisfied for any design solution, *optimal* requirements for which a maximal or minimal value of the index is required, *primary* requirements which take place in the specifications but can be modified to some extend to ensure a design solution, and *secondary* requirements which do not appear in the specifications but can be utilized to choose between multiple design solutions.

Ensuring the safety and complying with the ergonomic needs of the human operator are the two imperative design requirements every exoskeleton device must satisfy. Safety is typically assured by recruitment of back-drivable devices with force/torque limits implemented in software, while the ergonomic device design is considered at the kinematic synthesis level. The absence or avoidance of singularities within the workspace is another imperative design requirement, that ensures the forward and inverse kinematics of the robots be solved uniquely at each point within the workspace.

In this study, backdriveability of the device is assured by employing series-elastic actuators for the design. In addition to their low output impedances, implicit force measurements in these actuators allow for software torque limits to be implemented, offering further safety. The 3UPS configuration of the exoskeleton allows for ergonomic motion of human ankle over its RoM, since the ankle itself is a part of the kinematic structure. The 3RPS-R configuration works in a predetermined workspace that covers a large portion of the ankle workspace. Utilization of a passive revolute joint at the base platform of the device allows for intenal/external rotations of the foot. Further, customized trajectories and compliant couplings ensure ergonomic movements. The workspace of the 3RPS mechanism is selected to be free of singularities, while the redundant nature of 3UPS-RR kinematic structure is exploited for singularity avoidance.

The performance requirements to be optimized are highly dependent on the final use of the device. For a rehabilitation device that needs to bear human weight, the utilization from the actuators and the stiffness of the device should be maximized. In other words, the rigidity of the device and the torque output from the actuators should be the highest. Optimal performance of mechanisms are quantified through study of several design matrices, including scaled kinematic Jacobian (J) and mass (M) matrices. In this paper global performance measures, characterizing the performance of a manipulator over the entire workspace are considered.

To measure the performance of the rehabilitation device, two global condition indices, namely, average of local kinematic isotropy (AII) [30] and the minimum of minimum singular value (min $\underline{\sigma}$) of the scaled kinematic Jacobian matrix over the workspace. These optimizations are performed only for the 3RPS mechanism, since only in this configuration the exoskeleton is required to bear human weight; hence, the stiffness of the device and the utilization of the actuators are critical. An average value of the kinematic isotropy index is a sensible choice to characterize actuator utilization, since the use of worst-case performance indices imposes very conservative performance requirements. On the other hand, the minimum of the minimum singular value is still desired to be kept as high as possible over the workspace, since, the singularities of the Jacobian matrix correspond to lowest actuator utilization and device stiffness.

Since entries of kinematic Jacobian of the 3RPS mechanism is not homogenous in units, scaling factors are introduced to eliminate the physical units. The scaling is carried out through a transformation introduced by Stocco *et al.* [31], that normalizes the elements of the design matrices as fractions of their maximum values so that comparable relative values are ensured. In this study, the non-uniform force/torque requirements of the human ankle given in Table I is mapped to uniform forces at the joint space, since the actuators are selected to be identical.

The primary requirement for the wearable exoskeleton in 3UPS mode is selected as the volume index [29], the ratio between the workspace volume and the robot volume. Even though the 3RPS mechanism is optimized for best kinematical performance with the metrics introduced above, for the reconfigurable mechanism to function properly, the 3UPS mechanism must cover the whole RoM of the human ankle. Mild singularities may be tolerated within this workspace as the device is redundantly actuated. A large workspace volume index is also desirable to reduce the collisions of the device with the operator and the environment. The weight of the device is highly dependent on the selection of the actuators, more so than the link lengths; hence, there exists some flexibility on deciding the total mass of the kinematic structure.

Finally, the secondary requirements for the device include low backlash, low-friction, high back-drivability, and low manufacturing costs. Friction, backlash and back-drivability are required for good control performance and are mainly influenced by the selection of the actuators and the transmission. The choice of link lengths and the material may have an influence on manufacturing costs.

4. Optimization

4.1. Multi-criteria Optimization Problem

For optimal dimensioning of the exoskeleton as a rehabilitation robot, two objective functions characterizing the kinetostatic performance of the mechanism are considered. The objective of the optimization problem is to maximize the average kinematic isotropy of the mechanism (AII) while simultaneously maximizing the minimum of minimum singular value (min $\underline{\sigma}$) over the predetermined workspace. The optimization yields a Pareto-front curve that characterizes the trade-off between these performance indices.

The negative null form of the multi-objective optimization problem can be stated as

$$\begin{array}{c} \max\ \mathbf{F}(\boldsymbol{\alpha},\boldsymbol{\beta},\boldsymbol{\gamma}) \\ \mathbf{G}(\boldsymbol{\alpha},\boldsymbol{\beta}) \leq 0 \\ \mathbf{H}(\boldsymbol{\alpha},\boldsymbol{\beta}) = 0 \\ \boldsymbol{\alpha}_l < \boldsymbol{\alpha} < \boldsymbol{\alpha}_u \end{array} \tag{1}$$

where $\mathbf{F}$ represents the column matrix of objective functions that depend on the design variables $\boldsymbol{\alpha}$, parameters $\boldsymbol{\beta}$, and workspace positions $\boldsymbol{\gamma}$. Symbols $\mathbf{G}$ and $\mathbf{H}$ represent the inequality and equality constraint functions that also depend on design variables and parameters. Finally, $\boldsymbol{\alpha}_l$ and $\boldsymbol{\alpha}_u$ correspond to the lower and upper bounds of the design variables, respectively.

The symmetric 3RPS mechanism has two parameters $\beta_1 = R$ and $\beta_2 = \mathcal{W}$, where R is the radius of the fixed platform and is selected as 140mm according to statistical data on human joint sizes listed in Table II. $\mathcal{W} = \Psi_1 \times \Psi_2 \times h$ represents the predetermined workspace and is set as $\mathcal{W} = 40^\circ \times 36^\circ \times 50mm$ for the design of the ankle exoskeleton for balance/proprioception training. The optimization problem has two design variables: the ratio of the moving and base platform radii $\alpha_1 = r/R$ and the perpendicular distance of the moving platform $\alpha_2 = z$. Upper $\boldsymbol{\alpha_u}$ and lower $\boldsymbol{\alpha_l}$ limits on the design variables are imposed according to statistical data on human leg summarized in Table II.

The column matrix of objective functions for the haptic interface $\mathbf{F}$ is given as

$$\mathbf{F_{Rehab}} = \begin{bmatrix} min\ \underline{\sigma} \\ \frac{\int_{\mathcal{W}} \underline{\sigma}\,/\,\overline{\sigma}\, d\omega}{\int_{\mathcal{W}} d\omega} \end{bmatrix}$$

while the inequality and equality constraints $\mathbf{G}$ and $\mathbf{H}$ are imposed during kinematic analysis to ensure the closed kinematic chain for the 3RPS platform and the positive perpendicular travel pose of the mechanism, respectively. Due to space limitations, kinematic analysis of the 3RPS platform is not included in the paper, but a supplementary document is made available online [32].

4.2. Solution Method

The multi-criteria optimization of the 3RPS parallel mechanism is solved using the framework introduced in [33], [34]. This optimization framework for parallel mechanisms is based on NBI method [35] to efficiently obtain the Pareto-front hyper-surfaces characterizing the design trade-offs. This approach is computationally efficient, as the NBI method attacks the *geometric problem* directly by solving for single-objective constrained subproblems to obtain uniformly distributed points on the boundary of the feasible domain (Pareto-front hypersurface). Since the geometric problem is only affected by the properties of this hypersurface, the single-objective subproblems can be addressed using fast gradient based optimization

techniques even when the objective functions are non-smooth and non-convex. The approach is applicable to a general set of performance indices, and its implementation trivially extends to handle any number of objective functions. Moreover, the framework can solve for points on the non-convex regions of Pareto-front hyper-surfaces, a feature that is missing from the weighted sum methods.

The NBI method searches for a grid of uniformly distributed points to extract the geometry of the Pareto-front hypersurface. The method does not suffer from clumping of solution in the objective space and results in uniformly distributed points on the Pareto-front hyper-surface without requiring any tuning of the core algorithm. An increase in the number of points (resolution) of the grid that determines the number of solutions on the Pareto-front hyper-surface, maps to an almost linear increase in the computational time. Since the method assumes spatial coherence and uses solution of a subproblem to initialize the next subproblem, the convergence time for each subproblem may decrease for fine grids, resulting in further computational efficiency.

Limitations of the technique exist since the NBI method relies on an equality constraint. It is possible for the NBI method not to find a solution on the Pareto-front hyper-surface or converge to a local optima. In such a case, the solutions of NBI subproblems can be post processed to filter out undesired dominated solutions. The NBI method assumes sufficient smoothness of the boundary of the feasible domain so that gradient techniques can be employed; however, it has also been demonstrated in the literature that the method performs remarkably well even for non-smooth geometries of the objective space [36].

4.3. Implementation and Results

The NBI method requires one to specify the *shadow points*, the single criterion optimum of each objective function. Since the objective functions are non-convex and potentially non-smooth, the shadow points are calculated by a brute force search in both the parameter space and the workspace. For the nominal length, the parameter space is spanned from 200mm to 300mm, while the radii ratio is spanned from 0.2 to 0.8. The workspace is set as $\mathcal{W} = 40^\circ \times 36^\circ \times 50mm$. A fine discretization of the combined five dimensional vector space is used to achieve reliable estimates of the shadow points and over 3 million iterations are completed for each shadow point estimate. Iterations are time consuming as each iteration requires the configuration level kinematics of the parallel device to be solved. Unlike weighted sum methods, these searches are necessitated only once to calculate the shadow points for the NBI method. Once the shadow points are obtained, a much faster gradient-based optimization algorithm, namely SQP, is utilized to calculate the uniformly distributed set of non-dominated points on the Pareto-front curve.

The Pareto-front curve characterizing the trade-off between the average kinematic isotropy (AII) and the minimum of minimum singular value (min $\underline{\sigma}$) over the workspace of the 3R$\underline{\text{P}}$S mechanism is presented in Figure 2. From this plot one can observe that both AII and min $\underline{\sigma}$ vary an important amount for different values of design variables for the 3R$\underline{\text{P}}$S mechanism.

All of the points on the Pareto-front curve are non-dominated solutions of the multi-criteria optimization problem. A unique "optimal solution" can be selected from this set considering the primary objective and design thresholds on the performance requirements. For the 3U$\underline{\text{P}}$S configuration, the primary objective of the volume index is calculated for all of the solutions on the Pareto-front set. Specifically, a brute force workspace search of the 3U$\underline{\text{P}}$S mechanisms verified that, provided there exists a six DoF generalized force vector at the end effector of the mechanisms, not only the mechanisms can cover the whole RoM of the human ankle, but also the mechanisms never approach a singular configuration. Since all of the solutions on the Pareto-front set satisfies the required RoM, the volume index criteria simplifies down to the choice of a smaller device.

In addition to the primary objective, thresholds on the performance requirements are introduced in Figure 2 such that AII ≥ 0.45 and min $\underline{\sigma} \geq 0.55$. The thresholds are decided such that the compromise solution assigns comparable importance to both of the objectives. Outside the region determined by the thresholds, the deterioration in one of the objectives is far too high when compared with the gain in the other objective. It is important to note that the thresholds are introduced after the Pareto-front curve is generated and the trade-off between the competing criteria is carefully studied. Apriori assignment of such thresholds, without first gaining an insight into the trade-off, is prohibitive.

Given the thresholds and the primary objective an "optimal" design is selected with z = 300mm and r/R = 0.51. Since a well-distributed set of points characterizing the Pareto-front curve is already obtained, it is always possible to fit a curve to these points and estimate the percentage weight assigned to each performance criteria for any of the points lying on a convex sections of the Pareto-front curve[2]. Note that Pareto methods do not require apriori assignment of weights to the objective functions, although the assignment of such weights once the Pareto-front curve is formed may help decide between many non-dominated solutions. As a result of one such curve fit, the weight of the selected design is estimated as $\lambda = 0.43$.

Ten non-dominated solutions are calculated for the weighted sum approach using brute force search, in order to verify the weight estimated through the curve fit. Course discretization of the device workspace is used, since these calculations are very time consuming. Solutions of these weighted-sum problems are marked with "x"s in Figure 2. From these solutions, one can verify that the estimated weight is appropriate. Moreover, from the plot it is possible to observe that, as expected, the weighted-sum approach fails to find solution on the non-convex portions of the Pareto-front curve and results in a non-uniform distribution of (clamped) solutions, wasting the

[2]Weighted sum approaches fail to find solutions on the non-convex portions of the Pareto-front hypersurfaces.

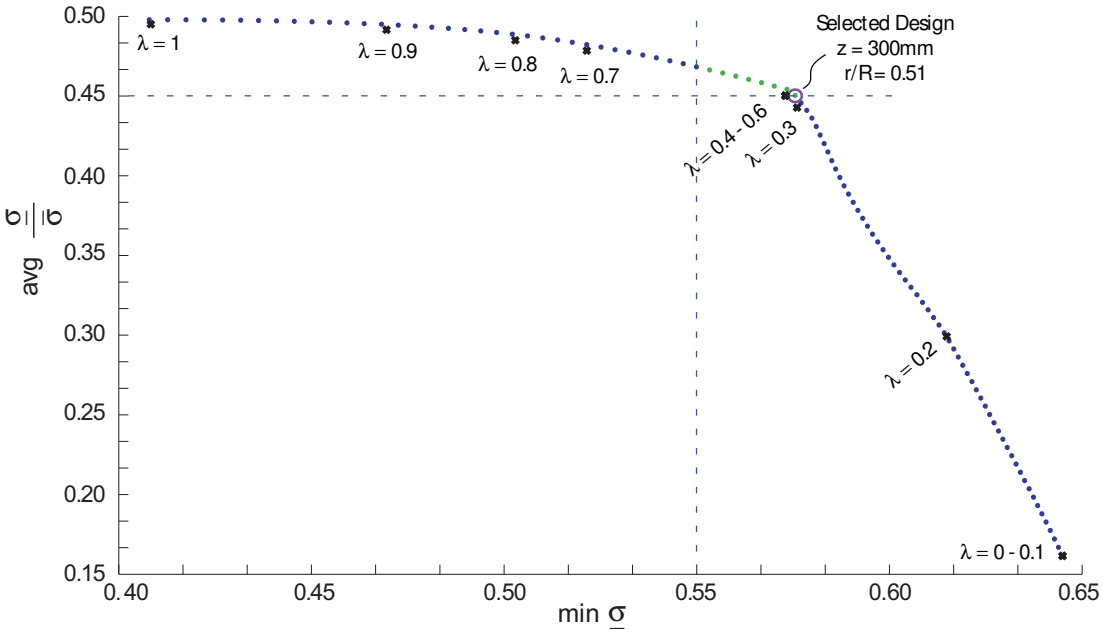

Fig. 2. Pareto-front Curve for min $\underline{\sigma}$ vs AII

computational effort.

5. Design of the Reconfigurable Exoskeleton

In Section II, the 3UPS-RR kinematic structure, which employs the human ankle as part of the kinematic chain, is proposed for RoM/strengthening exercises, while the 3RPS kinematic structure is proposed to support human weight during balance/proprioception training exercises. Both of the 3UPS and the 3RPS mechanisms need to be constructed using a fixed platform, a moving platform, and three actuated prismatic joints connecting these platforms. In both mechanisms the connections to the moving platform are made through spherical joints. The only difference between these two kinematic chains is how the prismatic joints are connected to the base platform. In particular, in the 3UPS mechanism prismatic joints are connected via universal joints, while revolute joints are used for the 3RPS mechanism. Extensive similarities between these two parallel mechanisms motivate the use of a single ankle exoskeleton device that can be arranged into both of these two mechanisms.

In this paper, a reconfigurable mechanism that can function as the 3UPS and the 3RPS manipulators is employed in the design of the ankle exoskeleton. The reconfiguration of the parallel manipulator to achieve different kinematic configurations, hence DoF, is achieved using interchangeable passive joint modules, as suggested in [37]. Reconfigurability embeds the ability to repeatedly change and rearrange the components of the system into the design in a cost efficient way [38], [39].

Interchangeable parts are indispensable components of rehabilitation devices to ensure ergonomy as well as hygiene. Many of the existing passive medical devices use several modules to target different physical therapy exercises. Nonetheless, the use of interchangeable joint and/or actuator modules to render different kinematic structures is not very common in robotic rehabilitation devices. Exceptions are the ankle rehabilitation device proposed by Yoon *et al.* [3] and a modular whole-arm therapy device proposed in [40]. In [3] reconfigurability is sought by changing and/or re-orienting several parts of the mechanism such that a ROM/strengthing exercise device can be also employed as a balance/proprioception device [16]. In [40], modular device designs allow therapy to be delivered for particular impairments with a stand-alone mode or as a whole-arm functional robot utilizing integrated modules.

Our device is similar to [16] in that reconfiguration is used to support both ROM/strengthing and balance/proprioception exercises. In our device, the reconfigurability is obtained through use of the lockable universal joints shown in Figure 3. When the joint is unlocked, series of revolute joints function as a universal joint rotating about the desired axes. When the second joint axis is locked using simple bolts, the locked universal joint is constrained to function as a revolute joint, that is free to rotate only about the first axis. Hence, the lockable universal joint allows a 3UPS mechanism to be reconfigured into a 3RPS mechanism, and visa versa.

Inspired by [3], another flexibility is added to the device through the foot plate which is designed with a lockable revolute joint. As a result MTP joint exercises, such as toe rise and heel rise, can also be performed with a simple reconfiguration of the device. The design of reconfigurable foot plate is depicted in Figure 4 in both locked and unlocked configurations.

In the final design, it is desirable to have a device that is wearable and portable, especially during balance/proprioception exercises. Using the optimal dimensions obtained in Section 4 and choosing 6061 aluminum as the material used for the links, the overall design weighs 4.9kg,

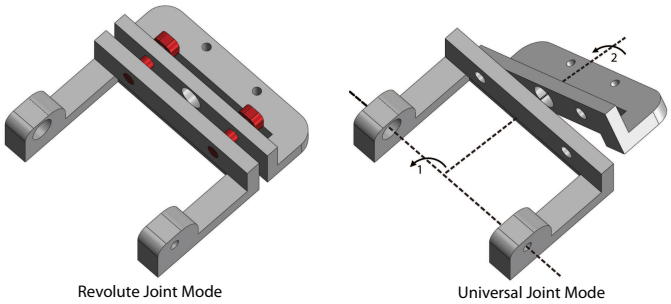

Fig. 3. Reconfigurable Universal/Revolute Joint

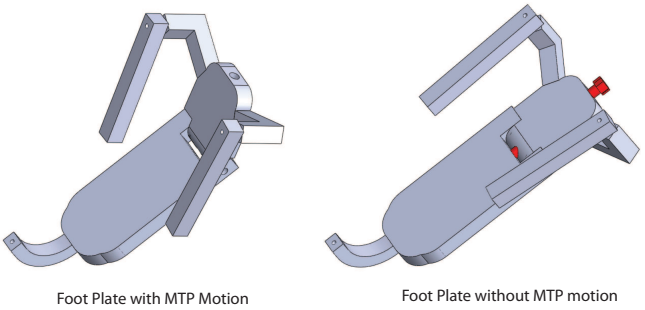

Fig. 4. Reconfigurable MTP Joint

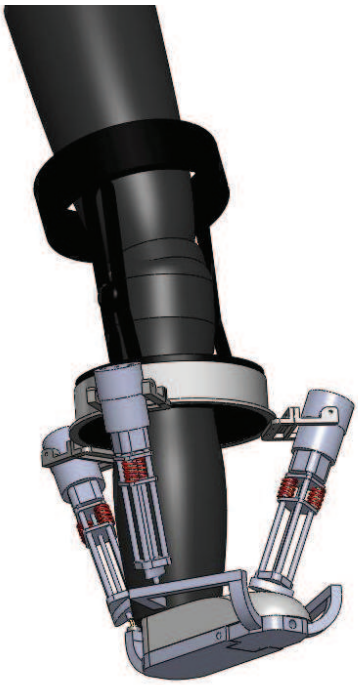

Fig. 5. *SUkorpion AR* in 3RPS Configuration

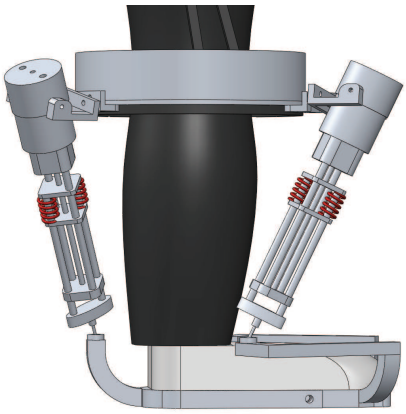

Fig. 6. *SUkorpion AR* in 3UPS Configuration

3.3kg of which is due to three series elastic actuators selected. The weight of the device is distributed over the upper leg and the upper mid-calf using tight straps around the knee as shown in Figure 5. Weight can further be distributed over the body by suspending the device from the shoulder of the operator, as done in [13].

The final design of the reconfigurable ankle rehabilitation robot, named *SUkorpion AR* after **S**abanci **U**niversity **K**inetostatically **O**ptimized **R**econfigurable **P**arallel **I**nterface **on** **A**nkle **R**ehabilitation, is presented in Figure 5 in 3RPS mode. An illustration of the robot in 3UPS mode is also given in Figure 6. Finally, in Figure 7 an early prototype of the device is presented which realizes the 3RPS-R mode with direct drive linear actuators.

6. Conclusions

The design and the optimal dimensional synthesis of a reconfigurable, parallel mechanism based ankle exoskeleton are presented. After identifying the relevant design criteria for the several physical therapy exercises, kinematic structures of mechanisms that are best suited for these applications are selected. A Pareto-front based multi-criteria optimization framework is applied to the dimensional synthesis of the exoskeleton device to study the trade-off between maximum stiffness and the actuator utilization. An "optimal" design is selected studying the trade-off curve and considering the primary and secondary design criteria. After the optimal dimensions of the device are decided, reconfigurability is embedded into the design such that the device can be arranged as a 3UPS manipulator to administer ROM/strengthing exercises and as a 3RPS manipulator to support balance/proprioception exercises. MTP joint exercises are also made possible through a reconfigurable design of the foot plate. Design details of the ankle exoskeleton, CAD snapshots, and an early prototype of the device are also presented.

Acknowledgments

The authors gratefully acknowledge the TÜBİTAK Grant 107M337 and the Marie Curie International Reintegration Grant 203324-REHAB-DUET.

References

[1] H. Tropp and H. Alaranta, *Sports Injuries: Basic Principles of Prevention and Care, Proprioception and coordination training in injury prevention.* Oxford, 1993.

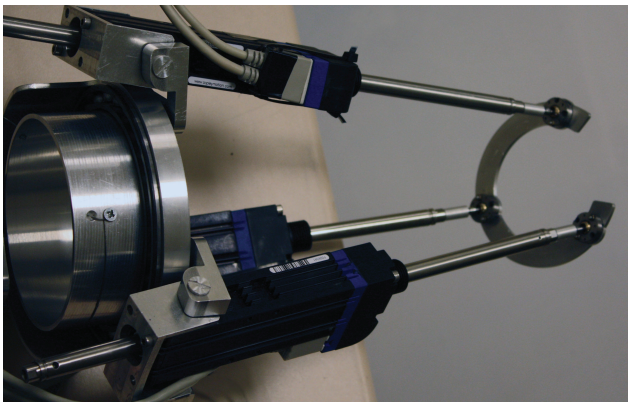

Fig. 7. Early prototype of *SUkorpion AR* in 3RPS Configuration

[2] D. Hung, M. Kennedy, A. Rowland, J. D. Purdy, and M. Yampolsky, "Ankle rehabilittaion: Evidence-based approach," Vanderbilt Rehabilitation Services.

[3] J. Yoon, J. Ryu, and K. Lim, "A novel reconfigurable ankle rehabilitation robot for various exercise modes," *Journal of Robotic Systems (Currently Journal of Field Robotics)*, vol. 22, no. 1, pp. 15–33, 2006.

[4] R. Ekkelenkamp, P. Veltink, S. Stramigioli, and H. van der Kooij, "Evaluation of a virtual model control for the selective support of gait functions using an exoskeleton," *Rehabilitation Robotics, 2007. ICORR 2007. IEEE 10th International Conference on*, pp. 693–699, June 2007.

[5] M. Girone, G. Burdea, and M. Bouzit, "The Rutgers Ankle orthopedic rehabilitation interface," in *Proceedings of the ASME Haptics Symposium*, vol. 67, 1999, pp. 305–312.

[6] M. Girone, G. Burdea, M. Bouzit, V. Popescu, and J. Deutsch, "Orthopedic rehabilitation using the Rutgers Ankle interface," in *Proceedings of Virtual Reality Meets Medicine 2000*, 2000, pp. 89–95.

[7] J. E. Deutsch, J. Latonio, G. Burdea, and R. Boian, "Rehabilitation of musculoskeletal injuries using the rutgers ankle haptic interface: Three case reports," in *Proceedings of Eurohaptics 2001*, July 1-4 2001, pp. 93–98.

[8] J. E. Deutsch, J. Latonio, G. C. Burdea, and R. Boian, "Post-stroke rehabilitation with the Rutgers ankle system: A case study," *Presence: Teleoper. Virtual Environ.*, vol. 10, no. 4, pp. 416–430, 2001.

[9] M. Girone, G. Burdea, M. Bouzit, V. Popescu, and J. E. Deutsch, "A Stewart platform-based system for ankle telerehabilitation," *Autonomous Robots*, vol. 10, no. 2, pp. 203–212, 2001.

[10] R. F. Boian, M. Bouzit, G. C. Burdea, J. Lewis, and J. E. Deutsch, "Dual Stewart platform mobility simulator," in *Proceedings of the ICORR 2005, 9th International Conference on Rehabilitation Robotics*, 2005, pp. 550–555.

[11] J. S. Dai, T. Zhao, and C. Nester, "Sprained ankle physiotherapy based mechanism synthesis and stiffness analysis of a robotic rehabilitation device," *Auton. Robots*, vol. 16, no. 2, pp. 207–218, 2004.

[12] A. Agrawal, S. Banala, S. Agrawal, and S. Binder-Macleod, "Design of a two degree-of-freedom ankle-foot orthosis for robotic rehabilitation," *Rehabilitation Robotics, 2005. ICORR 2005. 9th International Conference on*, pp. 41–44, June-1 July 2005.

[13] A. Roy, H. Krebs, S. Patterson, T. Judkins, I. Khanna, L. Forrester, R. Macko, and N. Hogan, "Measurement of human ankle stiffness using the Anklebot," *Rehabilitation Robotics, 2007. ICORR 2007. IEEE 10th International Conference on*, pp. 356–363, June 2007.

[14] C. E. Syrseloudis, I. Z. Emiris, C. N. Maganaris, and T. E. Lilas, "Design framework for a simple robotic ankle evaluation and rehabilitation device," *Engineering in Medicine and Biology Society, 2008. EMBS 2008. 30th Annual International Conference of the IEEE*, pp. 4310–4313, Aug. 2008.

[15] J. Yoon and J. Ryu, "A new family of hybrid 4-DoF parallel mechanisms with two platforms and its application to a footpad device," *Journal of Robotic Systems*, vol. 22, no. 5, pp. 287–298, 2005.

[16] ——, "A novel reconfigurable ankle/foot rehabilitation robot," *Robotics and Automation, 2005. ICRA 2005. Proceedings of the 2005 IEEE International Conference on*, pp. 2290–2295, April 2005.

[17] ——, "Design, fabrication, and evaluation of a new haptic device using a parallel mechanism," *IEEE Transactions on Mechatronics*, vol. 6, no. 3, pp. 221–233, 2001.

[18] USA Department of Defence, "Military handbook anthropometry of US military personnel (metric)," February 1991, DOD-HDBK-743A.

[19] X. Kong and C. M. Gosselin, "Type synthesis of 3-DoF spherical parallel manipulators based on screw theory," in *ASME Design Engineering Technical Conferences*, 2002.

[20] M. Karouia and J. M. Herve, "A family of novel orinetational 3-DoF parallel robots," in *CISM-IFToMM Symposium on Robot Design, Dynamics, and Control*, 2002, pp. 359–368.

[21] R. Di Gregorio, "Kinematics of a new spherical parallel manipulator with three equal legs: The 3-URC wrist," *Journal of Robotic Systems*, vol. 18, no. 5, pp. 213–219, 2001.

[22] I. A. Bonev and C. M. Gosselin, "Singularity loci of spherical parallel mechanisms," in *IEEE International Conference on Robotics and Automation*, 2005, pp. 2957–2962.

[23] K. M. Lee and D. K. Shah, "Kinematic analysis of a three degrees-of-freedom in-parallel actuated manipulator," *IEEE Transactions on Robotics and Automation*, vol. 4, no. 3, pp. 354–360, 1988.

[24] C. H. Liu and S. Cheng, "Direct singular positions of 3RPS parallel manipulators," *ASME Journal of Mechanical Design*, no. 126, pp. 1006–1016, 2004.

[25] A. Gupta and M. K. O'Malley, "Design of a haptic arm exoskeleton for training and rehabilitation," *IEEE Transactions on Mechatronics*, vol. 11, no. 3, 2006.

[26] A. Gupta, M. O'Malley, V. Patoglu, and C. Burgar, "Design, control and performance of RiceWrist: A force feedback wrist exoskeleton for rehabilitation and training," *IEEE Transactions on Robotics Research*, vol. 27, no. 2, pp. 233–251, February 2008.

[27] R. Unal and V. Patoglu, "Optimal dimensional synthesis of a dual purpose haptic exoskeleton," in *EuroHaptics '08: Proceedings of the 6th international conference on Haptics*, 2008, pp. 529–535.

[28] ——, "Optimal dimensional synthesis of force feedback lower arm exoskeletons," *Biomedical Robotics and Biomechatronics, 2008. BioRob 2008. 2nd IEEE RAS and EMBS International Conference on*, pp. 329–334, Oct. 2008.

[29] J. P. Merlet, *Parallel Robots*, 2nd ed. Springer, 2006.

[30] C. Gosselin and J. Angeles, "A global performance index for the kinematic optimization of robotic manipulators," *Journal of Mechanical Design*.

[31] L. Stocco, S. E. Salcudean, and F. Sassani, "Fast constrained global minimax optimization of robot parameters," *Robotica*, vol. 16, no. 6, pp. 595–605, 1998.

[32] A. Erdogan, A. C. Satici, and V. Patoglu, "Kinematic analysis of 3RPS mechanism - Supplementary document for REMAR 2009."

[33] R. Unal, G. Kiziltas, and V. Patoglu, "A multi-criteria design optimization framework for haptic interfaces," in *IEEE International Symposium on Haptic Interfaces for Virtual Environments and Teleoperator Systems*, 2008.

[34] ——, "Multi-criteria design optimization of parallel robots," in *IEEE International Conference on Cybernetics and Intelligent Systems and IEEE International Conference on Robotics, Automation and Mechatronics, CIS-RAM 2008*, 2008, pp. 112–118.

[35] I. Das and J. E. Dennis, "Normal-boundary intersection: A new method for generating the pareto surface in nonlinear multi-criteria optimization problems," *SIAM Journal on Optimization*, vol. 8, no. 3, pp. 631–65, 1996.

[36] E. Rigoni and S. Poles, "NBI and MOGA-II, two complementary algorithms for multi-objective optimizations," in *Practical Approaches to Multi-Objective Optimization*, 2005.

[37] A. K. D. I. M. Chen, S. H. Yeo, and G. Yang, "Task-oriented configuration design for reconfigurable parallel manipulators," *International Journal of Computer Integrated Manufacturing*, vol. 18, no. 7, pp. 615–634, 2005.

[38] R. Setchi and N. Lagos, "Reconfigurability and reconfigurable manufacturing systems: State-of-the-art review," *Industrial Informatics, 2004. INDIN '04. 2004 2nd IEEE International Conference on*, pp. 529–535, June 2004.

[39] M. Nourelfath, D. Ait-Kadi, and I. Soro, "Optimal design of reconfigurable manufacturing systems," *Systems, Man and Cybernetics, 2002 IEEE International Conference on*, vol. 3, pp. 6 pp. vol.3–, Oct. 2002.

[40] H. Krebs and N. Hogan, "Therapeutic robotics: A technology push," *Proceedings of the IEEE*, vol. 94, no. 9, pp. 1727–1738, Sept. 2006.